10 September 2024
alexander.forshay.thornton@cern.ch

Performance Study of the SND@LHC

Author: Alexander Thornton
Advisor: Simona Ilieva
CERN, Geneva, Switzerland

:

Summary

SND@LHC is a triggerless compact stand-alone experiment aiming to measure high energy neutrino cross section. The detector has nuclear emulsions, allowing for a detailed measurement of of neutrino interactions in an unexplored pseudo-rapidity range $7.2 < \eta < 8.4$. My project focused on event building from raw data sets and testing the parameters of employed event building strategies through many different analyses to further our understanding of the performance of the detector.

Contents

1 Introduction

1.1 Overview and Goals

The Scattering and Neutrino Detector at the Large Hadron Collider (SND@LHC) experiment at CERN focuses on studying high energy neutrinos, a type of particle created through collisions of protons within the LHC, and their probability of interacting with the material they pass through. This experiment is special because it studies neutrinos at energies never measured before (around 1 trillion electron volts) in a specific region of space that larger detectors cannot access. Located about 480m from where these collisions occur, namely the ATLAS collision point IP1, the SND@LHC experiment is shielded by over 100m of solid rock to ensure that only neutrinos (and muons, a closely related particle) can reach the detector. This specific setup allows researchers to exclusively observe neutrino interactions. Since neutrinos are extremely small and light particles, the SND@LHC target is made up of 800kg of the very dense material of tungsten to increase the probability of particle interactions. This tungsten is interleaved with many tiny detectors called nuclear emulsions that have exceptional spatial resolution which allows them to accurately capture the details of neutrino interactions. In particular the resolution allows researchers to clearly identify the interactions of a specific type of neutrino called the tau neutrino, due to the distinct features of the particle that the tau neutrino decays into.

The goal of my project was to optimize the way data is analyzed from the detector in a process called event building and to further test currently employed event building strategies. This is to ensure that all of the relevant physics such as neutrino interactions that the detector is looking for is present and not accidentally left or cut out.

1.2 Experimental Setup

The detector was developed to identify three neutrino flavors and search for feebly interacting particles as a potential dark matter candidate. The setup, shown on Figure 1, is composed of a target region where the particles enter that is followed downstream by a hadronic calorimeter and muon identification system. The detector is made up of four systems: The Veto planes, the Scintillating Fibre (SciFi) planes, the Upstream (US) planes and the Downstream (DS) planes. The Veto system rejects charged particles to reduce excessive background from passing-through muons and therefore allow neutrino interactions to be more easily observed. The SciFi system provides the timestamp of the neutrino interaction events within the detector and provide an energy measurement of electromagnetic showers. The US system provides a measurement of the hadronic showers, and the DS system serves as a muon identification system. [3]

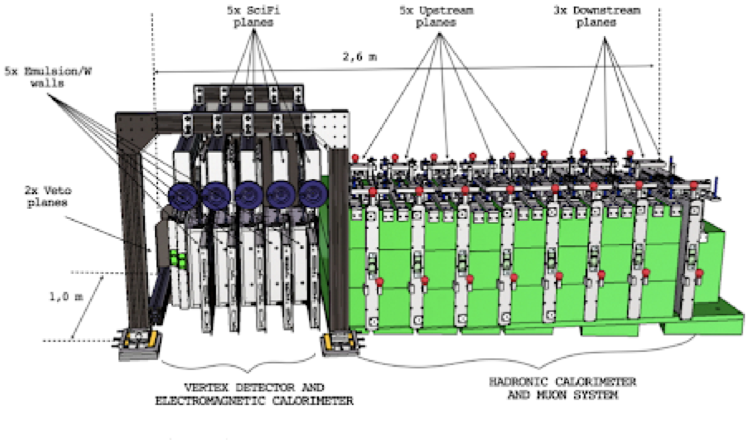

Figure 1: Experimental Setup of SND@LHC. [3]

2 Event Building

2.1 Event Building Process

Event building is the process of collecting, combining and organizing raw data from the detector into useful and understandable data that represents a particle interaction. The process of event building can be seen in Figure 2.

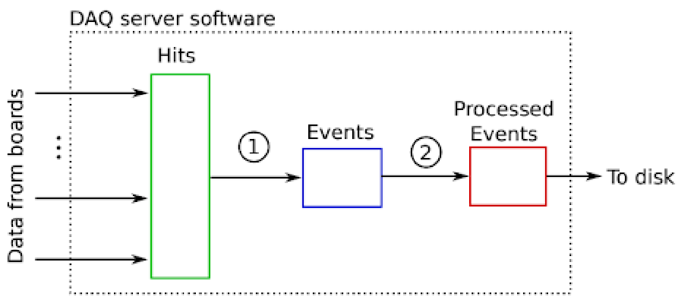

Figure 2: Event building process. [3]

First, the detector receives information from a particle interaction and stores its data, generally referred to as a “hit”. The information within a hit object is as follows: The TOF-PET chip that recorded the hit, the channel that recorded the hit, the Time-To-Analogue converter used for the calibration of the hit, the coarse and fine timestamp of the hit, and the coarse and fine value (corresponding to the deposited energy) of the hit. [4] The relevant information of a hit for my research is the coarse and fine timestamp of the hit, further explained in Section 3.1. All of the hits on all of the systems are then grouped together in intervals of 25ns, (this time period being determined by the clock cycle of the LHC), and these are called “events”. These events are then filtered and processed online, with many possible setting configurations but always including noise filtering. Finally, the events are written to a disk. [3]

2.2 Event Building for Each System

The first event building I completed was with the raw data from the LHC's 2022 proton run. I created 1D histograms for each individual system by plotting the amount of hits on the system over 25ns.

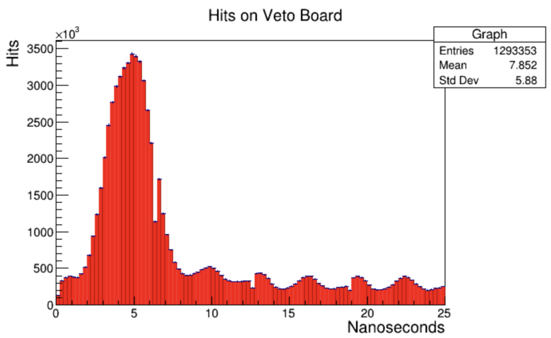

(a) 100,000 events of the Veto system with a peak around 7.5ns.

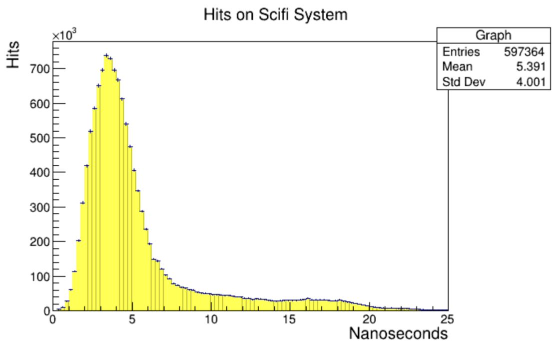

(b) 100,000 events of the SciFi system with a peak around 4.75ns.

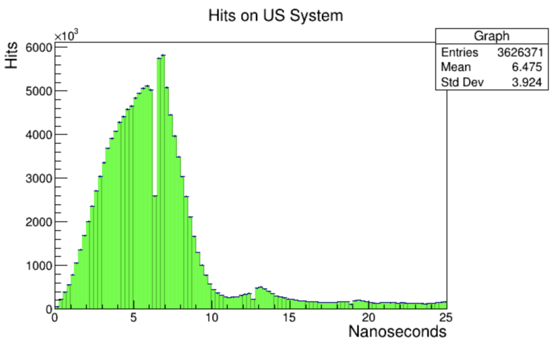

(c) 100,000 events of the US system with a peak around 6ns.

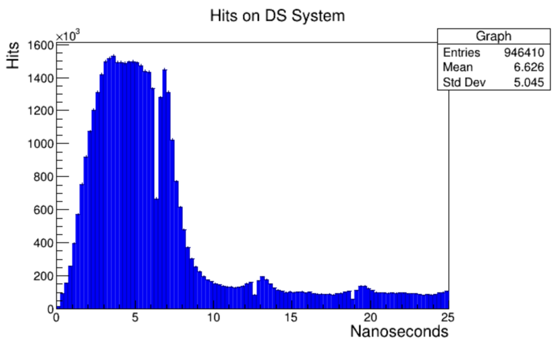

(d) 100,000 events of the DS system with a peak around 3-5ns.

Figure 3: Event building for each of SND@LHC's systems for the 2022 proton run.

The most striking part of these graphs are where there are small columns of missing data, most apparent in the US and DS systems. These "dips" in data are likely due to the difference in the discrete time measurements of the LHC's and SND@LHC's internal clock. The dips can be seen at regular intervals of 6.25ns. Correspondingly, the LHC's clock runs at 40Mhz (25ns), while SND@LHC's clock ticks exactly four times faster than that at 160Mhz (6.25ns). The data was likely "all pushed over" to just after each 6.25ns interval, creating the small dips and following artificial peaks that are easily seen in Figure 3a, Figure 3c, and Figure 3d.

Finally, I plotted a 2D histogram that shows the the timing information for each system compared to one another.

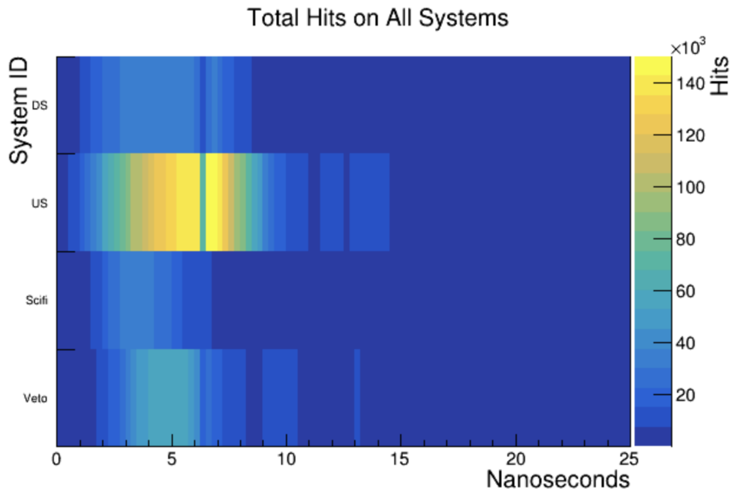

Figure 4: Hits on all systems over 100,000 events.

The y-axis shows each of the four systems, the z-axis shows the number of hits, while the x-axis is the timescale. The US system is hit much more than other systems over a slightly longer period of time because it has the largest surface area, followed by the Veto system, then finally the SciFi and DS systems. Once again it is possible to see the dip in data most starkly at 6.25ns as there is a consistent change in color (amount of hits) across the systems.

2.3 Event Building for Boards of Each System

Each system of the SND@LHC is read out by boards with individual ID numbers. The Veto system has only one board and is the smallest system, and the SciFi system has the most boards with 30. Knowing which boards of each system are being hit relative to each other in an event is important alongside the event building for the entire system. The following graphs show a deeper insight by breaking up Figure 3a - Figure 3d into their individual board components. (The Veto system is not included in these plots since it only contains one board, therefore a plot of this format would be identical to Figure 3a with only a visual difference.)

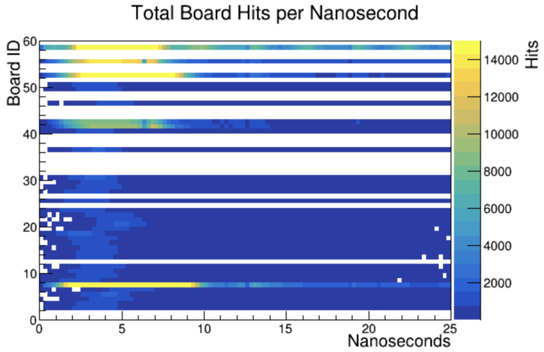

(a) Hits on all of the system's boards where boards 7, 55, 58, 60 are hit most frequently.

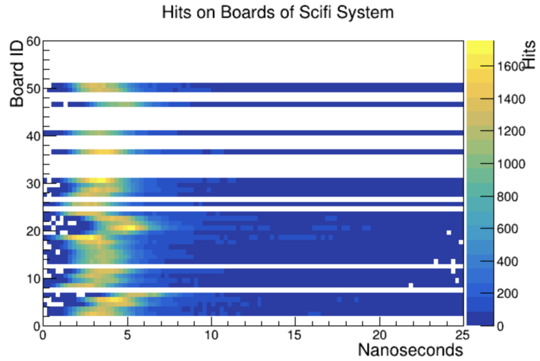

(b) Hits on SciFi boards where every board is consistently hit with similar peaks at similar times.

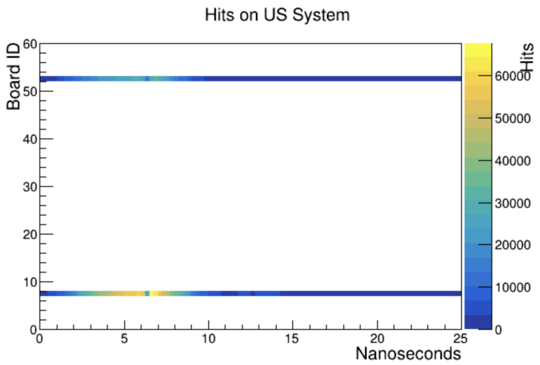

(c) Hits on US boards where board 7 is hit most frequently.

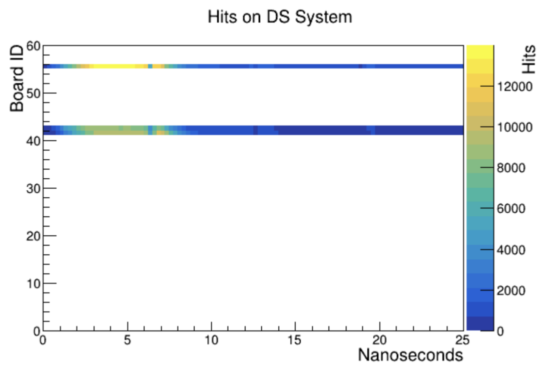

(d) Hits on DS boards where board 55 is hit most frequently.

Figure 5: Hits on individual boards for each system of SND@LHC.

These are 2D histograms where the y-axis is the specific board ID, the z-axis is the number of hits and the x-axis is the time of one event. The disparity in the amount of boards allocated to each system is easily apparent with SciFi containing the large majority, necessary to sustain the high spatial resolution provided by the detector for particles as they traverse the detector and to provide extremely accurate timestamps.

It is useful to know that all of the boards are being hit at a similar time across all systems, because it means that the systems are properly synchronized with one another. In 2022, the Veto system was out of sync with the other systems due to the physical implementation of boards, and this created challenges.

3 Investigation of Timestamps of Hits

3.1 Definition of Timestamps

To further investigate the dips in data first seen in Figure 3a - Figure 3d, it was necessary to learn more about how the timestamps of hits are calculated. The timestamp of a hit is calculated using both the coarse and fine timestamp. The coarse timestamp is a rough estimate of when the hit occurred. It is expressed in integer values of the SND@LHC clock cycle. The fine timestamp is a more precise measurement of when the hit occurred, and contains the raw value of the charge that is digitized by the Time-To-Digital Converters, defined within the interval of the coarse timestamp. Together, both timestamps define the time in which a hit occurred by first defining in which clock cycle the hit occurs (coarse timestamp) and then specifically when in that clock cycle the hit occurs (fine timestamp). The following equation is the mathematical definition to find the timestamp of a hit. [4]

$$\text{timestamp} = tc + f_{\text{TDC}}(\text{tf}, a, b, c, d) \tag{1}$$

where f_{TDC} is defined as:

$$f_{\text{TDC}}(x, a, b, c, d) = \frac{-b - \sqrt{b^2 - 4a(c - x)}}{2a} \tag{2}$$

The parameters a, b, c, and d depend on the previously mentioned TOFPET ID, channel, Time-To-Analogue Converter and Time-To-Digital Converter. These parameters are given and are calculated before data taking. [4]

3.2 Plotting of Coarse and Fine Event Timestamps

My goal was to investigate if the synchronization of event timestamps, made up of the coarse and fine timestamps, were causing the dips in data in the event building. To do so I overlaid two normalized event building graphs of the US system over one another, Figure 3c and a graph of the same events but using only coarse timestamps instead of event timestamps.

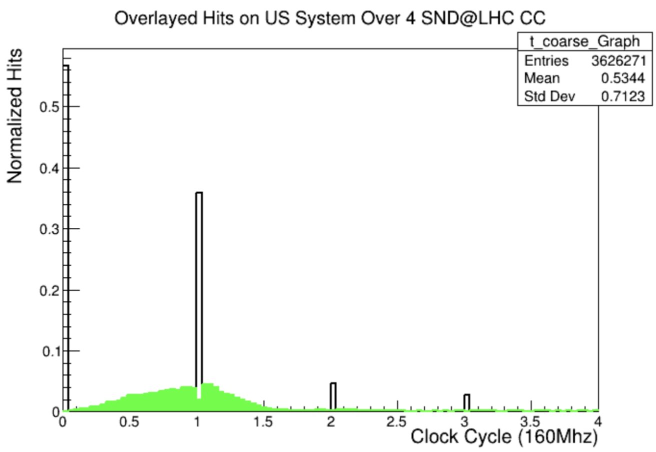

Figure 6: Overlaid normalized event building graphs using event timestamp in green and coarse timestamp in black.

This graph contains the SND@LHC clock cycle on the x-axis (still over an entire length of 25ns as previously done as each SND@LHC clock cycle is 6.25ns), and the hits on the y-axis. One will notice the y-axis has fractional hits which isn't physically possible. This is because the graph has been normalized in an effort to better compare the data between event timestamp and coarse timestamp.

It is clearly shown that the coarse timestamps appear at every SND@LHC clock cycle where the original dips in data occurred. This shows the effect of the timing calibration used to determine the hit timestamp. Finding ways to smooth this distribution is beyond the scope of this research, but it was important to identify the reason behind the observed dips.

4 Testing Efficiency of Existing Event Building Script

4.1 Testing Event Building Script's Noise Filters

The next part of my research was testing the parameters of already employed event building techniques. To begin, I had to install the necessary software, compilers and modules to be able to successfully run the DAQ server and then the following event building script. The script is a manager that can loop over many possible runs with many specific predetermined parameters including the noise filters, maximum event duration, hit gap, and clock alignment.

The first part of this project was to test the different possible noise filter configurations. This is very important because noise filters are essential in clearing out useless data so that the useful physics we are searching for is visible. The script had two types of noise filters, for convienence labeled as follows: a dual noise filter (DNF) that was comprised of a fast noise filter and an advanced noise filter, and a combined noise filter (CNF) that joined the fast and advanced filters together. I ran the script under the exact same parameters and changed only which noise filter was used for each run, and found the data to be perfectly identical.

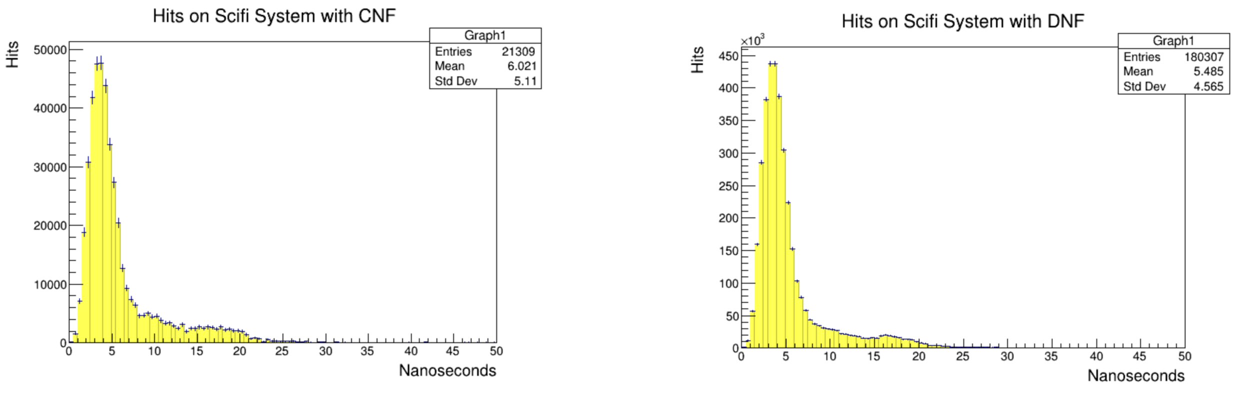

(a) 100,000 events in the SciFi system using the script and combined noise filter (CNF).

(b) 100,000 events in the SciFi system using the script and the dual noise filter (DNF).

Figure 7: Comparing the combined and dual noise filters through event building.

These plots were created with the exact same event building parameters, except for the difference in noise filter arragement. These graphs are exactly identical as seen in the data boxes in the top right, confirming that both of the noise filters are accurate and equal.

4.2 Testing Parameters of Event Building Script

The next step of the script was to test the event building configuration parameters in an attempt to further investigate the raw data and then see if there is any noticeable inefficiency in the event building. The most important parameter to change was the maximum event duration. I therefore ran the script with this value at 4 and 8, corresponding to 4 and 8 SND@LHC clock cycles (CC). This was then compared to the initial event building I did previously in Figure 3a - Figure 3d to check that there are no drastic changes in the raw data. Below is the comparison of the SciFi graphs and total graphs for both parameters.

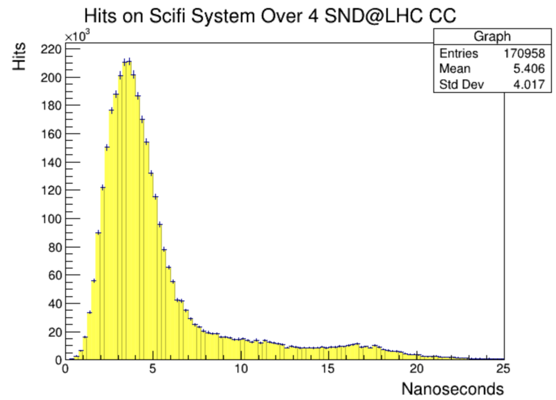

(a) 100,000 events in the SciFi system over 4 SND@LHC clock cycles.

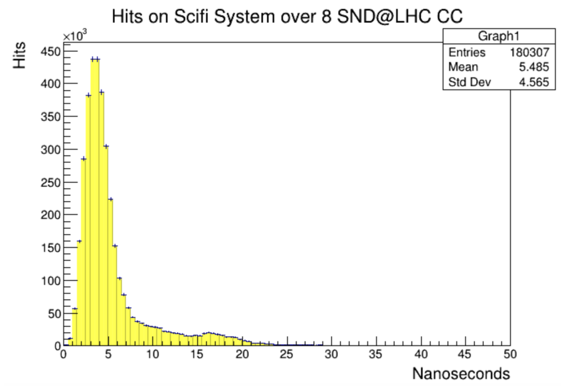

(b) 100,000 events in the SciFi system over 8 SND@LHC clock cycles.

Figure 8: Comparing the different lengths of event building in the SciFi system.

These plots are very similar, as seen both visually and by the mean value in the statistics box in the top right. Notice that there are about twice as many hits on the graph with 8 SND@LHC clock cycles because the event duration is twice as long. This is expected since more events with SciFi activity will pass the noise filters given the longer event duration. This signifies that there are no drastic changes on the raw data level even though we increase the event duration, a necessary data point to verify. The next graphs shown will be a 2D plot of all systems plotted against one another with the different event durations.

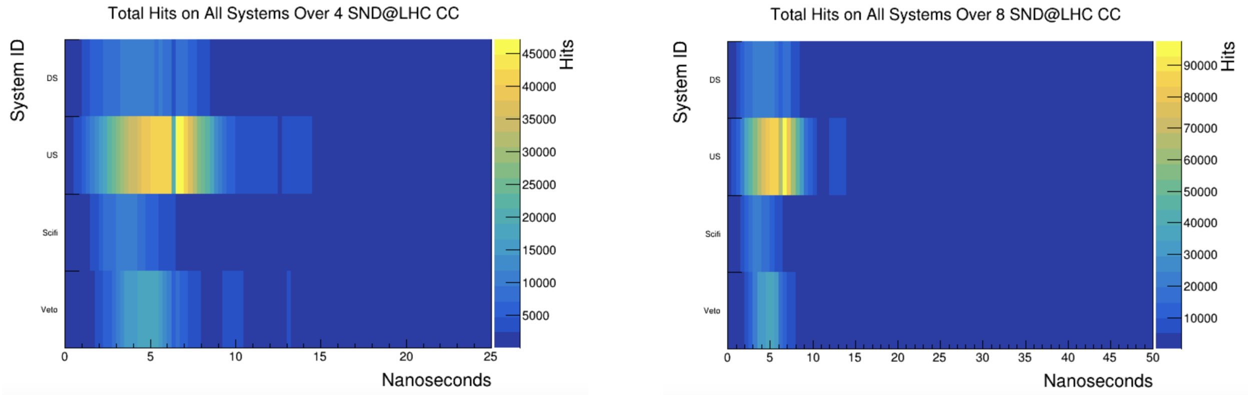

(a) 100,000 events over all systems over 4 SND@LHC clock cycles.

(b) 100,000 events over all systems using 8 SND@LHC clock cycles.

Figure 9: Comparing the different lengths of event building across all systems.

Once again these are the expected plots as they show similar trends of when the hits are detected, and there are more total hits in the event that is twice as long. There is seemingly no meaningful data from the 25-50ns range for the longer event, so using a longer event in this specific analysis is not particulary more useful.

4.3 Using Event Building Data to Further Investigate the SND@LHC's Parameters

I used the newly created event building data files over 4 and 8 SND@LHC clock cycles to further investigate the QDC values, total number of hits and time alignment of the detector. Investigating these parameters under the new data files is useful since we can further analyze and understand the data of the parameter we are exploring alongside the original event building script itself. I began this process by plotting the QDC (Charge to Digital Converter) values for both event duration settings. By analyzing the QDC values one can assess how efficiently the detector detects and records signals for different energies.

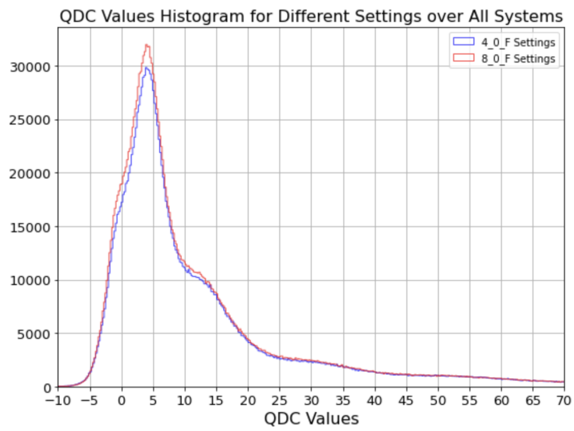

Figure 10: QDC Values for 4 (blue) and 8 (red) SND@LHC clock cycles from event building script overlaid.

The first number in 4_0_F and 8_0_F translates to 4 or 8 SND@LHC clock cycles, the second value translates to the hit_gap = 0 and the third value translates to setting align_with_clock=false in the event building parameters. The y-axis is the unit-less count of occurrences of the QDCs that have that x-axis value. The different structures on this plot correspond to the different systems, with the small shoulder around 10-15 QDC originating in the Veto system. The expected amount of charge received by the QDCs should be smooth increase and decrease with an obvious peak. Next, I plotted a 1D histogram of the total number of hits over multiple events for both 4 and 8 SND@LHC clock cycles overlaid onto one another in an attempt to see how different the hit distribution would be for different lengths of events.

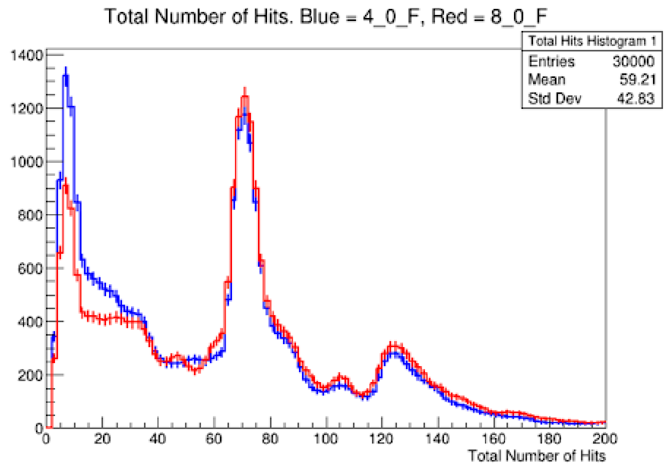

Figure 11: Total number of hits across multiple events and all systems, for 4 (blue) and 8 (red) SND@LHC clock cycles.

The x-axis contains the total number of hits while the y-axis is the count of occurrences for the corresponding total number of hits. The two graphs are largely overlaid similar onto one another, with the large difference being that there are more occurrences for the total number of hits in the 4 SND@LHC clock cycle graph between 5-35 total number of hits. This is expected result and due to the shorter length of the events. The 8 SND@LHC clock cycle events capture more data, leading to the mitigation of the peak at smaller hit counts.

Next, I tested the difference of event timestamps of consecutive events in an attempt to gain a better understanding of the performance and timing of the event building data over 4 and 8 SND@LHC clock cycles.

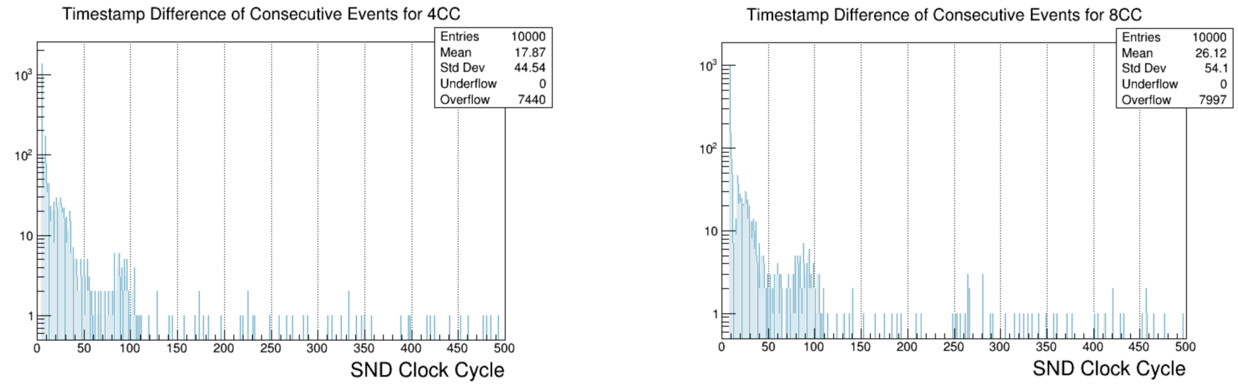

(a) The timestamp difference of consecutive events for 4 SND@LHC clock cycles.

(b) The timestamp difference of consecutive events for 8 SND@LHC clock cycles.

Figure 12: Comparing timestamp differences of different event building lengths.

The x-axis is the timestamp difference between events in terms of SND@LHC clock cycles, while the y-axis is the count of occurrences of how many timestamps had that specific difference between events on a logarithmic scale. There should theoretically be no difference between the timestamp differences of consecutive events, but due to the nature of hardware and electronics there are always exceptions. In the graphs we observe that at first there is no large difference between the different settings. Next, the largest block of data is between the 0-100 SND@LHC clock cycles, with a sharp peak near 1000 occurrences at around 10 SND@LHC clock cycles. This is a very good result, generally saying that most events do not have large differences in their timestamps. There are outliers above 100 SND@LHC clock cycles, which can be partially attributed to to an inefficiency due to detector dead time.

Finally, I investigated the time aligment of boards with respect to the LHC (via a 160MHz bunch number) for different event building parameters. Protons in the LHC beam are grouped into “bunches”, packets of protons with a finite length. For reference, in 2017 there were a maximum 2556 bunches of 1.15×10^{11} protons per bunch at 6.5 TeV. [2]

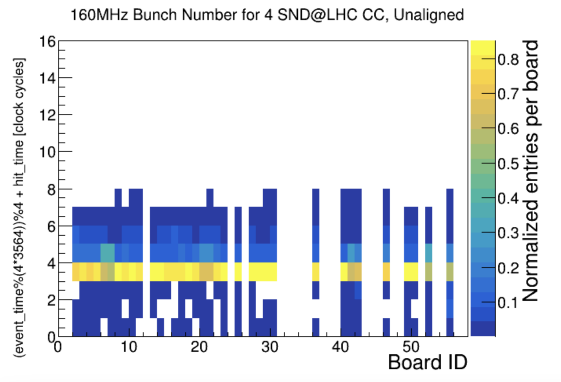

(a) Graph of 160MHz bunch number over 4 SND@LHC clock cycles and not aligned.

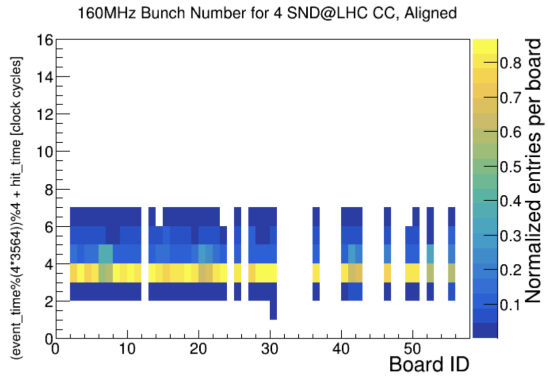

(b) Graph of 160MHz bunch number over 4 SND@LHC clock cycles and aligned.

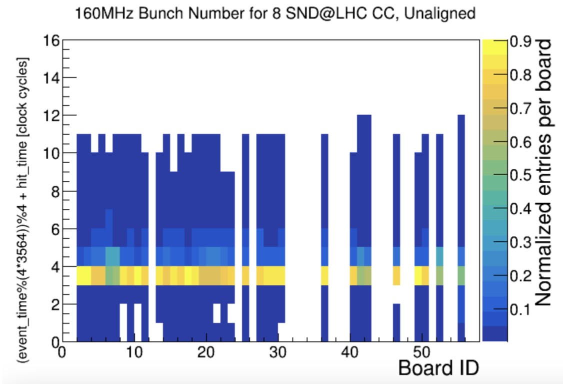

(c) Graph of 160MHz bunch number over 8 SND@LHC clock cycles and not aligned.

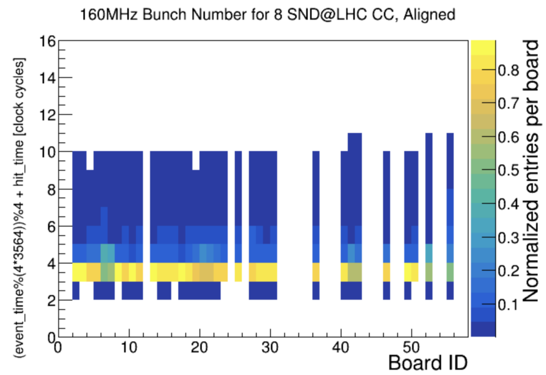

(d) Graph of 160MHz bunch number over 8 SND@LHC clock cycles and aligned.

Figure 13: Graphs of 160MHz bunch number over different event building parameters.

The y-axis is an equation of time given by (event_time $\%(4 \times 3564))\,\%4 +$ hit_time [clock cycles] that aligns the events of the LHC and the SND@LHC clock together so that we can see the alignment of the hits. The x-axis is the specific board ID that has been hit while the z-axis is the normalized hits on the boards. The yellow strip observed corresponds to the most probable time that the boards are hit. All the boards are hit very equally at a very similar time. Setting the event building parameter that aligns the detector clock with the LHC, shown in the graphs with "Aligned" in the title, produces better data by taking out unnecessary noise. Therefore, this is a preferred event building parameter choice. The difference between the 4 and 8 SND@LHC clock cycle event building parameter choice in these graphs is small. The 8 SND@LHC clock cycle event has more data stretched over a long time, but the amount of hits in this longer time is negligible. Therefore there is no preferred length of event building parameter for these graphs.

5 Working in Emulsion Laboratory

5.1 Ordering Emulsions for Processing System

I worked in a laboratory dark room to prepare SND@LHC's nuclear emulsions for processing. The emulsions in the detector act as the tracking devices for particles with micrometric accuracy. The processing system analyses the whole thickness of the emulsion, acquiring tomographic images at equally spaced depths by moving the focal plane along the vertical axis. [3]

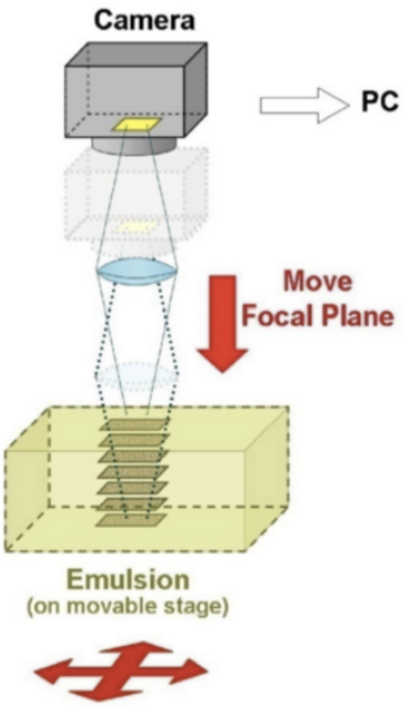

(a) Schematic drawing of the scanning procedure [3].

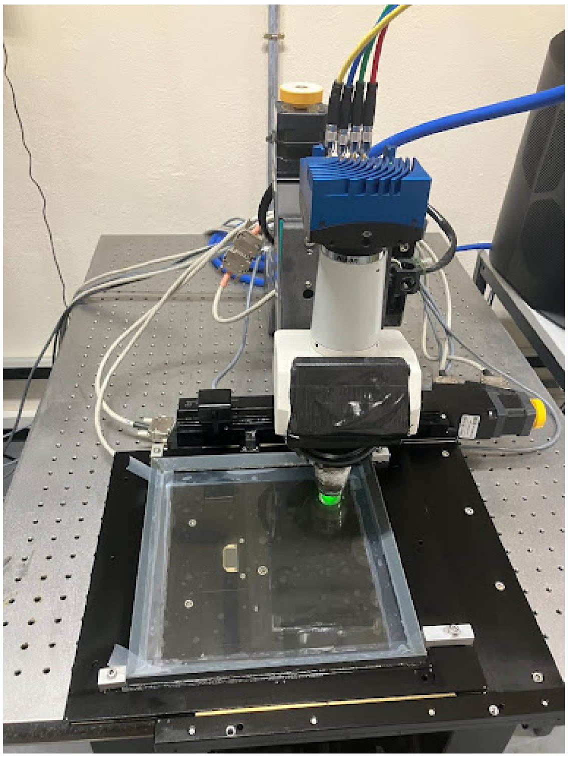

(b) Optical microscope used for the SND@LHC emulsion film scanning (taken by me, July 30, 2024).

Figure 14: Photo and diagram of the emulsion scanning process.

Before the scanning procedure can begin, the emulsions must be removed from the detector in the LHC tunnel and transported to the laboratory dark room. There, they are ordered and prepared before being sent to a nuclear emulsion lab and placed in a chemical solution to develop visible, permanent tracks. After this, they can be processed in light as shown in Figure 14b. In the dark room, we began by allowing our eyes to adjust to the darkness and blocking any remaining light sources, such as door cracks. Therefore, of course, taking photos while working in the dark room was impossible. Using extremely dim red headlamps, we ensured minimal light exposure while working. Our team consisted of three members. One person removed the emulsions and tungsten from the detector and handed the emulsions to the other two team members, which included myself. We then verified the numbers on the emulsions to ensure they were correctly ordered, matching their positions in the detector for accurate processing. After verification, we packaged the emulsions in light-proof film. Once this was completed, we sent the emulsions to another lab for chemical development to form the permanent tracks.

6 Muon Tracking Script and Analysis

6.1 2D Distributions of Start Positions

The next step was to take the event building data that I had created and convert it to the offline software format to run muon tracking over the SciFi and DS systems so that I could use SND@LHC software classes during my analysis. The muon tracking analysis was done over many different event building parameters which created many graphs that were extremely similar. Therefore I will show the muon tracking analysis over the same event building parameters. Namely, over 8 SND@LHC clock cycles and with the detector time-aligned to the LHC. The rest of the graphs using different event building parameters can be explored in Appendix A. The first muon tracking parameter that I explored was the 2D spatial distribution of the muon's start positions in the transverse plane as they entered the detector.

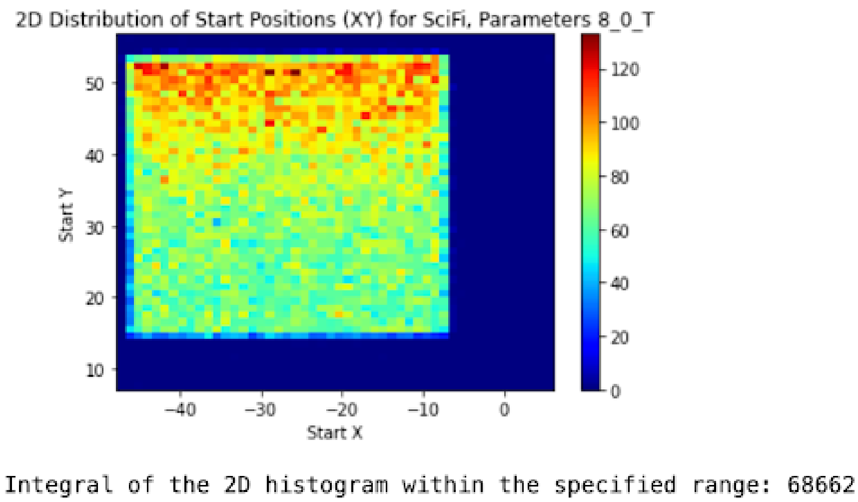

Figure 15: Graph of 2D start positions of muons entering the SciFi system hitting the top of the detector most frequently.

The x-axis and y-axis of the graph show the physical size of the detector. For SciFi, the ranges for the detector are $-42\,\text{cm} \leq x \leq -11\,\text{cm}$ and $18\,\text{cm} \leq y \leq 49\,\text{cm}$. The z-axis is the amount of hits of muons the SciFi system experiences. It is observed that the SciFi system is getting hit very consistently, with an increase of hits towards the top of the detector. The integration of all of the bins within the SciFi system is performed to eventually calculate the muon flux. Next, the same plot is done over the DS system.

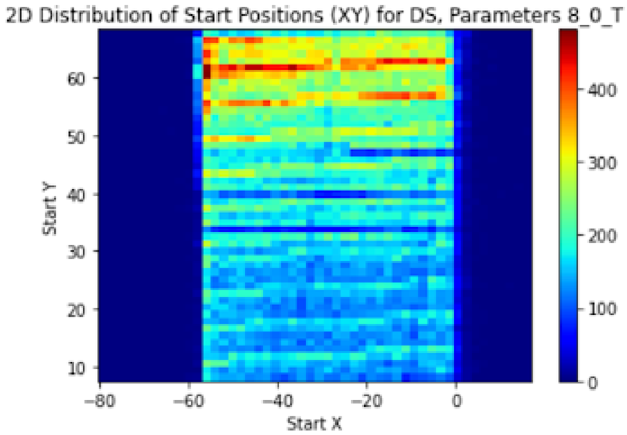

`Integral of the 2D histogram within the specified range: 211713`

Figure 16: Graph of 2D start positions of muons entering the DS system and showing the structure of the systems bars.

For DS, the ranges for the detector are $-54\,\text{cm} \leq x \leq -2\,\text{cm}$ and $12\,\text{cm} \leq y \leq 64\,\text{cm}$. The darker bars show tracking inefficiency due to bar registration inefficiency. This is because of an alignment issue between the bars and their readout that was taken care of in the 2022 yearly technical stop of the LHC.

6.2 Muon Flux Calculation

Now that I had analyzed the distribution of the start positions of the muons, I did calculations to find the muon flux through the SciFi system, defined as Φ_μ:

$$\Phi_\mu = \frac{N_{\text{real tracks}}}{\text{integrable area} \times \text{luminosity}}$$

where

$$N_{\text{real}} = \frac{N_{\text{counted tracks}}}{\text{efficiency}}$$

Where $N_{\text{real tracks}}$ is the number of real tracks, $N_{\text{counted tracks}}$ is the number of counted tracks and efficiency is the detection efficiency. The number of $N_{\text{counted tracks}}$ is the integration of the bins within the detector's area. The efficiency of SciFi tracking was taken from Reference [1]. The integrable area is simply the area of the detector, where the tracking efficiency is uniform [1]. That left the luminosity variable which was provided by the ATLAS collaboration. I then propagated the error throughout the calculation and discovered for my data that the muon flux $\Phi_\mu = 2.06 \pm 0.008\,(\text{stat}) \pm 0.07\,(\text{sys}) \times 10^4\,\text{fb/cm}^2$ with a relative uncertainty of 5.4%. I then compared this value to previous literature and discovered that a previous SciFi muon flux value that used the same tracking as me but different event building parameters found $\Phi_\mu = 2.06 \pm 0.01\,(\text{stat}) \pm 0.012\,(\text{sys}) \times 10^4\,\text{fb/cm}^2$ with a relative uncertainty of 6% [1]. The extreme similarity between the two muon fluxes is an incredible result, it proves that SND@LHC has robust event building code and that results can be similarly reproduced. The small decrease in uncertainty in my calculation can be attributed to the additional third source of uncertainty considered in Reference [1], namely the tracking method used. In this study I only used Hough Transform tracking, see Reference [1] for more details.

6.3 2D Distributions of Slopes

The next muon tracking parameter I explored was the distribution of slopes of the muon tracks.

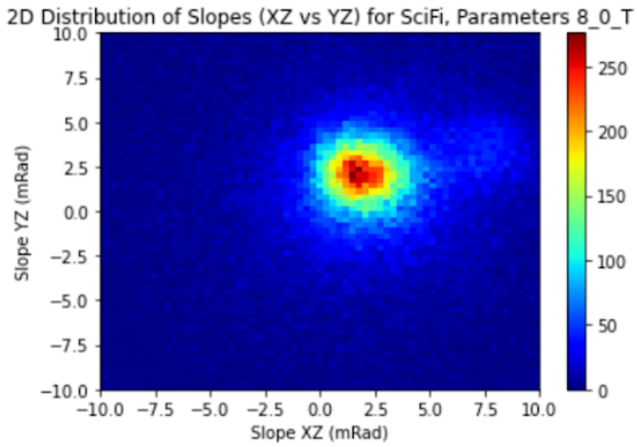

Figure 17: Graph of 2D slope distribution of muon tracks in the SciFi system.

The x-axis and y-axis make up the slope of the muon tracks in milliradians, while the z-axis is the amount of tracks with that specific slope. The SciFi system has very high resolution and is therefore very precise when making muon measurements. Most of the slopes of the tracks are contained within 0-5 milliradian xz-slope and yz-slope, as the largest number of tracks are around 2.5 milliradian xz-slope and yz-slope. I then performed this analyis upon the DS system.

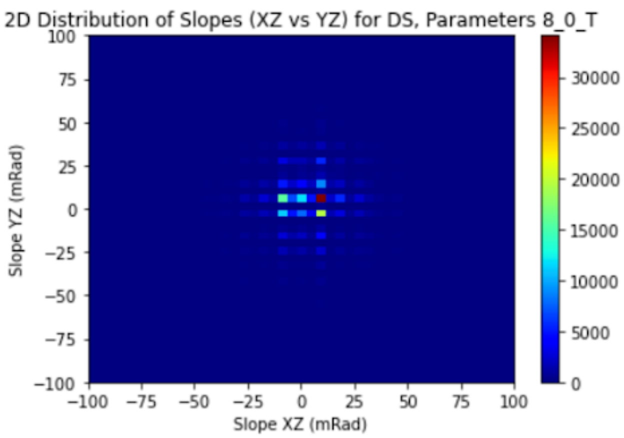

Figure 18: Graph of 2D slope distribution of muon tracks in the DS system.

The DS system has a much lower resolution than SciFi (I use around a factor of 1000 less bins) with a larger area. Therefore it is possible to make out the individual horizontal and vertical bars that make up the DS system. Furthermore, the detector acceptance of the DS system is larger, so there are a larger amount of tracks in comparison with the SciFi system.

6.4 1D Distributions of Track Quality

The last set of muon tracking parameters I analyzed with my event building data was the track quality. The track quality is a measure of how well a reconstructed particle track fits the expected behavior of the particle moving through the detector.

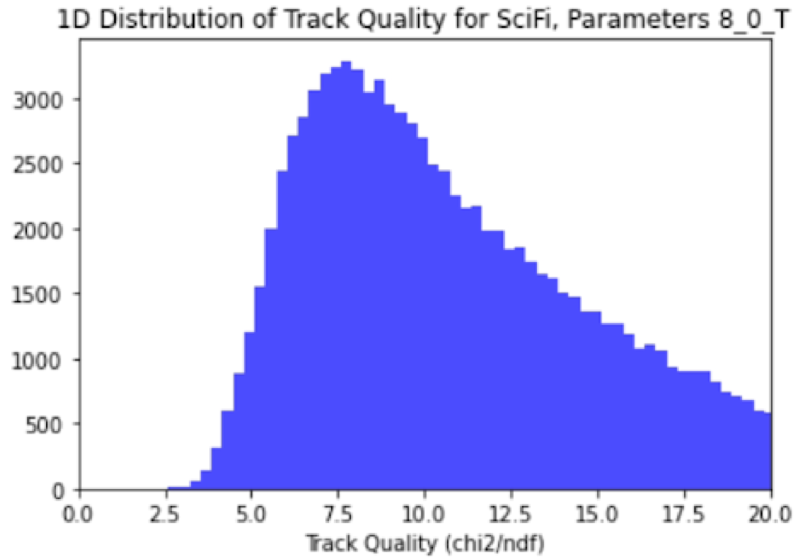

Figure 19: Graph of the muon track quality in the SciFi system.

The x-axis is the unit-less statistical measure of track quality which is expressed as χ^2/ndf, where χ^2 is a statistic measuring the difference between observed data and expected model, while ndf are the degrees of freedom the track has. The y-axis are the amount of occurrences there are at a specific track quality value. The reason why the x-axis values are shifted with respect to 0 is because we supply a track fitter with hits within a spatial tolerance of 0.1cm of the pattern recognition (the Hough Transform) line prediction. See details in Reference [1]. Finally, I perform the same analyis on the DS system.

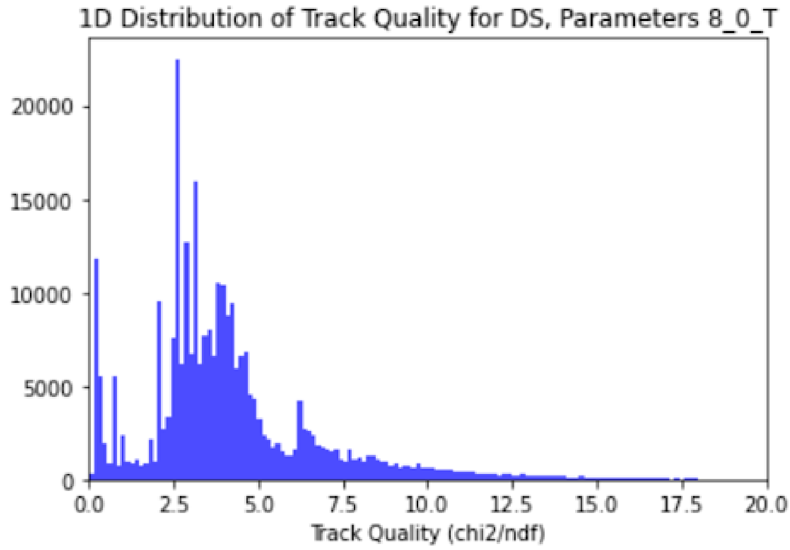

Figure 20: Graph of the muon track quality in the DS system.

For the DS system we see discrete spikes in the track quality which are a manifestation of the larger granularity of this detector system (the bar size is 1x1 cm^2.

7 Conclusion

My research was performing event building and testing parameters of current event building strategies and applying it to many types of analyses to do an overall performance study on the SND@LHC detector. This was largely done through the investigation of the timestamps of events, testing different noise filters, determining the efficiency of employed event building scripts, and muon tracking. I discovered that there are dips in the event building data due to the effect of the timing of calibration used to determine the hit timestamp, and therefore created a new potential research investigation to smooth out this data. I confirmed that two currently employed noise filter settings work as intended. I worked in the laboratory and assisted in removing the nuclear emulsions from the detector. I discovered results in terms of the muon flux measurement showing that the employed event building is robust. The last step that I could not complete due to timing constraints is the Veto inefficiency study. However, my data will be used to run a manager that will produce such an estimate out of the box.

A Appendix A

All of the following graphs are the same analysis done in the Muon Tracking and Analysis section, but for the other event building parameters.

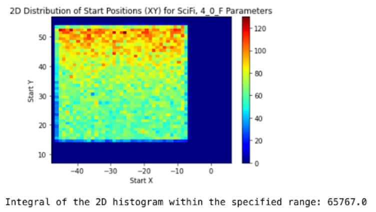

(a) 4 SND@LHC clock cycles and align_with_clock=false

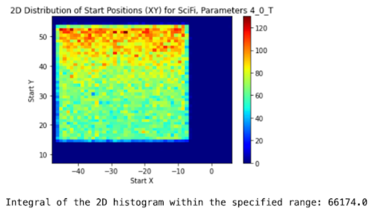

(b) 4 SND@LHC clock cycles and align_with_clock=true

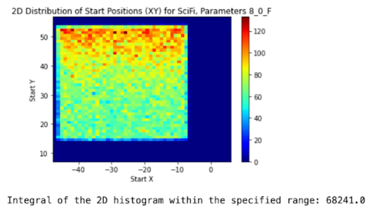

(c) 8 SND@LHC clock cycles and align_with_clock=false

Figure 21: Start positions of muon tracks in SciFi system over multiple event building parameters.

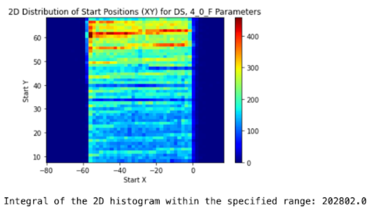

(a) 4 SND@LHC clock cycles and align_with_clock=false

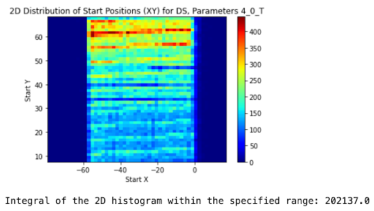

(b) 4 SND@LHC clock cycles and align_with_clock=true

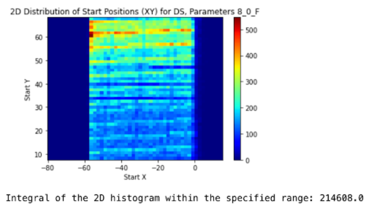

(c) 8 SND@LHC clock cycles and align_with_clock=false

Figure 22: Start positions of muon tracks in DS system over multiple event building parameters.

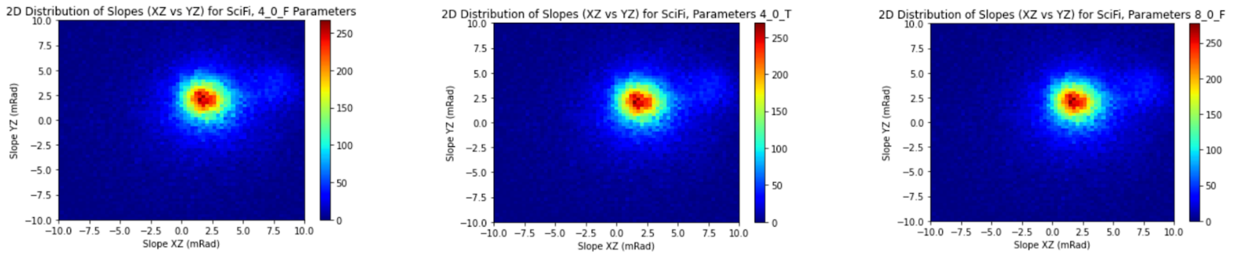

(a) 4 SND@LHC clock cycles and align_with_clock=false

(b) 4 SND@LHC clock cycles and align_with_clock=true

(c) 8 SND@LHC clock cycles and align_with_clock=false

Figure 23: Slope distributions over SciFi system over multiple event building parameters.

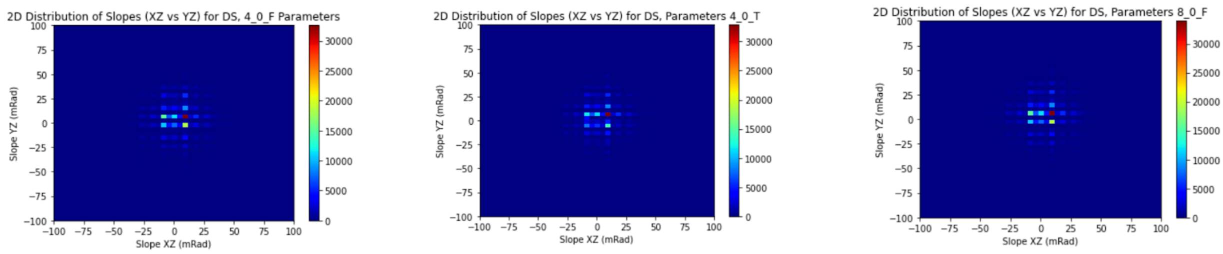

(a) 4 SND@LHC clock cycles and align_with_clock=false

(b) 4 SND@LHC clock cycles and align_with_clock=true

(c) 8 SND@LHC clock cycles and align_with_clock=false

Figure 24: Slope distributions over SciFi system over multiple event building parameters.

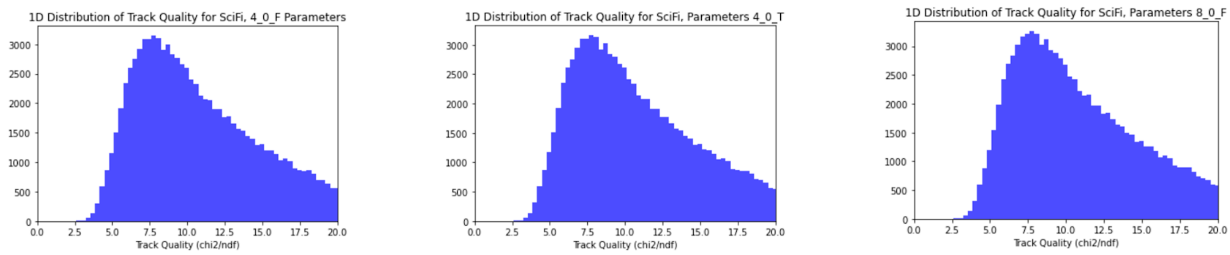

(a) 4 SND@LHC clock cycles and align_with_clock=false

(b) 4 SND@LHC clock cycles and align_with_clock=true

(c) 8 SND@LHC clock cycles and align_with_clock=false

Figure 25: Track quality over SciFi system over multiple event building parameters.

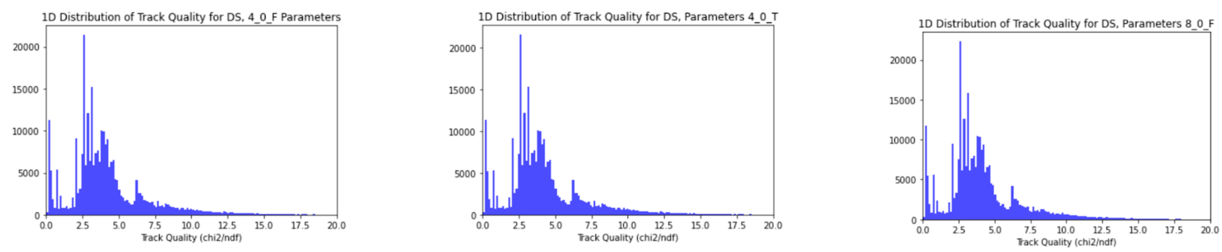

(a) 4 SND@LHC clock cycles and align_with_clock=false

(b) 4 SND@LHC clock cycles and align_with_clock=true

(c) 8 SND@LHC clock cycles and align_with_clock=false

Figure 26: Track quality over DS system over multiple event building parameters.

References

[1] R. Albanese, A. Alexandrov, F. Alicante, et al. Measurement of the muon flux at the snd@lhc experiment. *Eur. Phys. J. C*, 84:90, 2024.

[2] CERN. Lhc report: A full house for the lhc, 2024. Accessed: 2024-08-05.

[3] LHC Collaboration. Snd@lhc: The scattering and neutrino detector at the lhc, 2023.

[4] Ettore Zaffaroni. SND-SciFi Software Wiki: Raw Data Format. https://gitlab.cern.ch/snd-scifi/software/-/wikis/Raw-data-format, 2024. Accessed: 2024-07-04.